jmr&t Journal of Materials Research and Technology

www.jmrt.com.br

Original Article

Stored energy in ultrafine-grained 316L stainless steel processed by high-pressure torsion☆

Moustafa El-Tahawy[a,b], *Yi Huang*[c], *Taekyung Um*[d], *Heeman Choe*[d], *János L. Lábár*[a,e], *Terence G. Langdon*[c], *Jenő Gubicza*[a,*]

[a] *Department of Materials Physics, Eötvös Loránd University, Budapest, Hungary*
[b] *Department of Physics, Faculty of Science, Tanta University, Tanta, Egypt*
[c] *Materials Research Group, Faculty of Engineering and the Environment, University of Southampton, Southampton, United Kingdom*
[d] *School of Materials Science & Engineering, Kookmin University, Seoul, Republic of Korea*
[e] *Institute for Technical Physics and Materials Science, Centre for Energy Research, Hungarian Academy of Sciences, Budapest, Hungary*

ARTICLE INFO

Article history:
Received 10 April 2017
Accepted 6 May 2017
Available online 19 June 2017

Keywords:
High-pressure torsion
Stored energy
Stainless steel
Phase transformation
Thermal stability

ABSTRACT

The energy stored in severely deformed ultrafine-grained (UFG) 316L stainless steel was investigated by differential scanning calorimetry (DSC). A sample was processed by high-pressure torsion (HPT) for $N = 10$ turns. In the DSC thermogram, two peaks were observed. The first peak was exothermic and related to the annihilation of vacancies and dislocations. During this recovery, the phase composition and the average grain size were practically unchanged. The energy stored in dislocations was calculated and compared with the heat released in the exothermic DSC peak. The difference was related to the annihilation of vacancy-like defects with a concentration of $\sim 5.2 \times 10^{-4}$. The second DSC peak was endothermic which was caused by a reversion of α'-martensite into γ-austenite, however in this temperature range dislocation annihilation and a moderate grain growth also occurred. The specific energy of the reverse martensitic phase transformation was determined as about -11.7 J/g.

1. Introduction

316L austenitic stainless steel has a great importance in many practical applications. Due to its high strength, good ductility, high fracture toughness, excellent corrosion resistance and low absorption rate of neutron radiation, 316L is used as a structural material in nuclear power plants and, also, in biomedical applications such as orthopedic implants [1–4]. In order to improve the mechanical performance of 316L steel, severe plastic deformation (SPD) procedures are often applied on coarse-grained specimens [5–8]. One of the most effective SPD method in grain refinement is high-pressure torsion (HPT) [9–12]. It was shown that HPT processing of 316L steel yielded ultrafine-grained (UFG) or even nanocrystalline microstructure with a very high dislocation density [5,6,8]. The grain

☆ Paper was a contribution part of the 3rd Pan American Materials Congress, February 26th to March 2nd, 2017.

* *Corresponding author.*
E-mail: jeno.gubicza@ttk.elte.hu (J. Gubicza).

http://dx.doi.org/10.1016/j.jmrt.2017.05.001

refinement in 316L austenitic stainless steel to a nano-scale through SPD is often accompanied by a phase transformation from face-centered cubic (fcc) γ-austenite to body-centered cubic (bcc) α′-martensite structure with a transition sequence γ-austenite → ε-martensite → α′-martensite [5,6,8]. Although the α′-martensite structure is harder than γ-austenite, the high fraction of α′-martensite phase in steels may yield an easier corrosion and intergranular embrittlement [7,13]. Therefore, there is a demand to obtain UFG microstructure in 316L steel while maintaining the fcc austenitic structure.

It was reported that the heat treatment of plastically deformed stainless steels can result in a reverse martensitic phase transformation which may yield a UFG austenitic microstructure with improved mechanical properties [14–18]. It was also revealed that the stability of α′-martensite and the mechanisms of reverse transformation depend on the heat treatment conditions and the chemical composition of stainless steels [19–22]. Stainless steels usually possess a low stacking fault energy (SFE) with values of 20–40 mJ/m^2, however the concentrations of alloying elements (e.g., Cr, Ni, Mn, Mo and Al) have a strong influence on the value of the SFE [19,23–26]. For instance, the addition of Al considerably increases SFE in 316L steel, which stabilizes γ-austenite during SPD and facilitates the reverse martensitic transformation during annealing [19]. In addition, the SFE has a significant effect on both the deformation mechanisms occurring during SPD and the stability of the UFG microstructures in subsequent annealing processes [27]. The lower the SFE, the easier the occurrence of deformation twinning. Moreover, the low SFE is accompanied by a low twin boundary energy, therefore the nucleation of new grains bounded by twin boundaries is easier during annealing, thereby facilitating the recrystallization of the UFG microstructures.

The thermal stability of the phase composition and the UFG microstructure in stainless steels are very important from the point of view of their practical applications since their changes may considerably alter the functional (e.g., mechanical and corrosion) properties. The stability is significantly influenced by the energy stored in lattice defects (e.g., in vacancies, dislocations and grain boundaries) in SPD-processed materials. Although numerous reports have been published on the evolution of the phase composition and the grain size in UFG stainless steels during heat treatments [14,15,28,29], the change of the energies stored in vacancies, dislocations and grain boundaries versus annealing temperature has not been studied. In this work, the evolution of the stored energy in nanocrystalline 316L steel processed by 10 turns of HPT was studied as a function of annealing temperature by differential scanning calorimetry (DSC). A former investigation indicated that after 10 turns a saturation state of the microstructure was achieved [8]. For the calculation of the energies stored in dislocations and grain boundaries, the dislocation density and the grain size were determined as a function of annealing temperature by X-ray line profile analysis (XLPA) and electron microscopy, respectively. Since a reverse martensitic phase transformation also occurred during annealing, the fractions of α′-martensite and γ-austenite phases were also monitored during the DSC scan. The energies of vacancies and reverse transformation were estimated indirectly from the difference between the measured and calculated stored energies.

2. Experimental material and procedures

The studied material was a 316L austenitic stainless steel with an alloying element composition of 17.20% Cr – 8.97% Ni – 2.13% Mo – 1.03% Mn – 0.77% Si – 0.48% Cu – 0.35% Co (in wt.%), as determined by energy dispersive X-ray spectroscopy. The initial material was annealed at 1373 K for 1 h and then quenched to room temperature (RT). As a result of this process, the initial material was an almost single phase γ-austenite with a mean grain size of ~42 μm [8]. Disks with thicknesses of ~0.85 mm were processed by 10 turns of HPT operating under quasi-constrained conditions [30,31], with an applied pressure of 6.0 GPa at room temperature (RT). The evolution of the microstructure, the phase composition and the hardness during HPT processing were studied in detail in an earlier investigation [8].

The change in the stored energy during annealing of the HPT-processed sample was studied experimentally by DSC. For calorimetry measurements, small pieces were cut from the peripheral regions of the HPT disk. To avoid the oxidation during DSC annealing, the experiments were carried out under an Ar atmosphere in a Perkin Elmer (DSC2) calorimeter at a heating rate of 20 K/min. The maximum temperature of the DSC scans was 1000 K. After the first scan, the measurement was repeated as the second thermogram can facilitate the determination of the baseline. The change of the stored energy was determined experimentally from the heat released or absorbed in the DSC peaks, which were obtained after baseline subtraction. The experimentally determined released/absorbed heat values were compared with the changes of the stored energy calculated from the variation of the phase composition and the lattice defect structure during annealing. For studying the changes of the microstructure and the phase composition during heat treatment, samples were annealed up to characteristic temperatures in the thermograms at a rate of 20 K/min and then quenched to RT. These specimens were mechanically polished using a 2500 grit silicon carbide paper and then the surfaces were electro-polished using an electrolyte with a composition of 70% ethanol, 20% glycerine and 10% perchloric acid (in vol.%) in order to remove the uppermost surface layer distorted due to mechanical polishing.

The fraction of γ-austenite in the samples annealed up to different temperatures was measured by X-ray diffraction (XRD). The XRD patterns were obtained by a high-resolution diffractometer using Co$K_{\alpha 1}$ radiation (wavelength: $\lambda = 0.1789$ nm). X-ray line profile analysis (XLPA) was also performed on the same diffractograms by the Convolutional Multiple Whole Profile (CMWP) fitting method [32] in order to determine the dislocation density (ρ) in the major phase. In this method, the diffraction pattern is fitted by the sum of a background spline and the diffraction profiles obtained as the convolution of the instrumental and microstructural peaks. The CMWP evaluation of the parameters of the dislocation structure requires the knowledge of the average dislocation contrast factors ($\bar{C}_{hkl}$), characterizing the dependence of diffraction peak broadening on the indices of reflections *hkl*. The average contrast factors for cubic polycrystals are given as [33]:

Table 1 – The values of $\bar{C}_{h00}$ and q for edge and screw dislocations for both γ-austenite and α′-martensite phases of 316L stainless steel.

Structure	Anisotropic elastic constants [GPa]			Edge		Screw	
	c_{11}	c_{12}	c_{44}	$\bar{C}_{h00}$	q	$\bar{C}_{h00}$	q
α′-Martensite	248	110	120	0.205	0.55	0.276	2.51
γ-Austenite	210	130	120	0.281	1.53	0.289	2.33

$$\bar{C}_{hkl} = \bar{C}_{h00}\left(1 - q\frac{h^2k^2 + k^2l^2 + h^2l^2}{\left(h^2 + k^2 + l^2\right)^2}\right), \quad (1)$$

where $\bar{C}_{h00}$ is the contrast factor for reflection $h00$ and parameter q describes the edge/screw character of dislocations. The values of $\bar{C}_{h00}$ and q are not available in the literature but they can be determined from the anisotropic elastic constants of the different phases in 316L stainless steel. The anisotropic elastic constants are $c_{11} = 210$, $c_{12} = 130$ and $c_{44} = 120$ GPa, and $c_{11} = 248$, $c_{12} = 110$ and $c_{44} = 120$ GPa for γ-austenite and α′-martensite phases, respectively [34–36]. These values were used for the determination of $\bar{C}_{h00}$ and q for the two phases using the software ANIZC [33]. The calculation was carried out for both edge and screw dislocations. The values obtained for $\bar{C}_{h00}$ and q are listed in Table 1. In γ-austenite with fcc structure, besides the parameters of the dislocation structure, the twin-fault probability (β_t) was also evaluated by the CMWP fitting method [34]. This quantity gives the fraction of twin faults among {111} planes in the fcc structure.

In the sample processed by HPT and the specimens annealed at or below 950 K, the grain size was very small, therefore transmission electron microscopy (TEM) investigations were performed to determine the grain size for the calculation of the energy stored in high-angle grain boundaries (HAGBs). These TEM investigations were carried out using a Philips CM-20 transmission electron microscope operating at 200 keV. The TEM foils were thinned first by mechanical grinding to a thickness of 50 μm and then they were ion milled using an Ar ion beam at an inclination angle of 5° until perforation. The ion milling was conducted at 7 keV and 2 mA with continuous cooling of the sample by liquid nitrogen. In the samples heated up to 1000 K, the grain size increased to sufficiently large values for their investigation by scanning electron microscopy (SEM) using an FEI Quanta 3D microscope. Electron backscatter diffraction (EBSD) images were taken with a step size of 40 nm and evaluated using OIM software (TexSem Laboratories). The grain size was determined by the OIM program considering only those boundaries which have misorientations higher than 15°.

3. Experimental results

3.1. *DSC investigation of the initial material and the sample processed by HPT*

Fig. 1 shows DSC thermograms for the initial material and the peripheral part of the disk processed by HPT for $N = 10$ turns. For the initial sample, only one small exothermic DSC peak was observed in the temperature range between ~580 and ~770 K. The area under this peak was ~1.3 J/g. At the same time, two characteristic DSC peaks were observed for the HPT-processed specimen. The first, exothermic peak developed between ~580 and ~740 K, which is similar to the temperature range observed for the initial material. However, the released heat, estimated as the area under the exothermic peak, increased from ~1.4 J/g to ~4.9 J/g due to 10 turns of HPT. For the sample processed by HPT, a second, endothermic peak was also detected between ~740 and ~950 K. Such an endothermic peak was not observed for the initial material. The area under the endothermic peak was −5.7 J/g for $N = 10$ revolutions. The processes occurring in the temperature ranges related to the DSC peaks were analyzed by studying the change of the phase composition and the microstructure upon annealing. For this purpose, samples were annealed up to the starting and end temperatures of the DSC peaks (see Fig. 1) and then they were quenched to RT. The microstructures and the phase compositions of these specimens were compared. These results are presented in the next section.

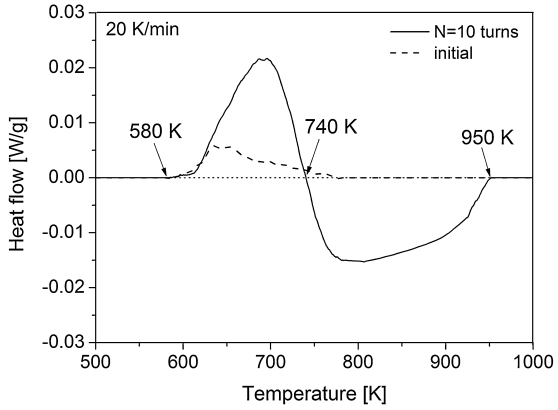

Fig. 1 – DSC thermograms obtained at a heating rate of 20 K/min for the initial material and the peripheral part of the disk processed by HPT for $N = 10$ turns.

3.2. *Evolution of the phase composition and the microstructure during annealing*

The phase compositions and the microstructures of the initial material and the sample processed by HPT for $N = 10$ revolutions were documented previously in detail [8]. It was found that the initial specimen exhibited a coarse-grained microstructure with an average grain size of ~42 μm. This material was an almost single phase γ-austenite with a very small fraction of α′-martensite (~3%). Due to HPT-processing, γ-austenite was transformed to ε- and α′-martensites and after 10 turns the main phase was α′-martensite with a fraction of ~74%, as estimated from the integrated intensities

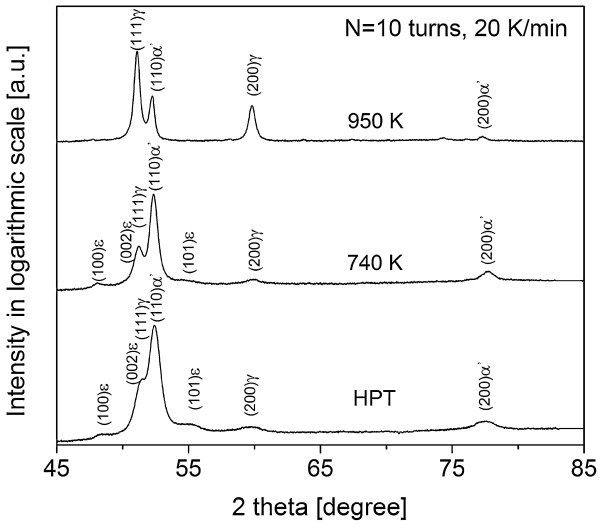

Fig. 2 – X-ray diffraction patterns taken on the HPT-processed sample and after annealing at different temperatures. The indices of reflections are indicated above the peaks.

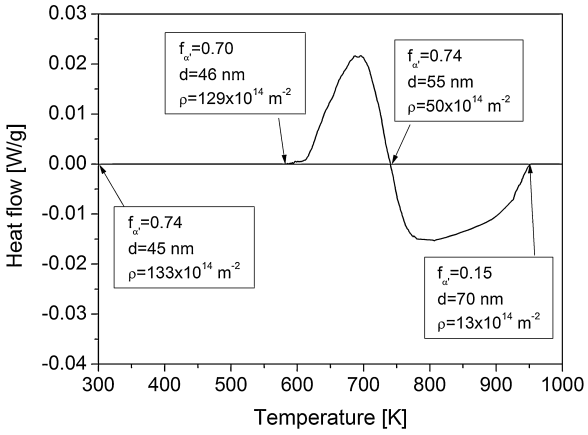

Fig. 3 – The fraction of α′-martensite ($f_{\alpha'}$) obtained by XRD, the dislocation density (ρ) in the main phase determined by XLPA and the average grain size (d) obtained by TEM for the HPT-processed sample and the specimens annealed up to the beginning and the end of the exothermic peak and the end of the endothermic peak. The corresponding DSC thermogram is also shown.

under the XRD peaks. The grain size was refined to ~45 nm at the periphery of the disk processed by $N = 10$ revolutions. In addition, the dislocation density increased to $\sim 133 \times 10^{14}\ m^{-2}$ in the main α′-martensite phase.

The change of phase composition during DSC annealing was determined by XRD. The integrated area under the XRD peaks was used to estimate the fractions of the different phases. It was found that the initial material remained a nearly single phase γ-austenite during annealing up to 1000 K. Fig. 2 shows parts of the XRD patterns obtained for the periphery of the HPT disk processed for $N = 10$ turns and after annealing at various temperatures. The XRD peaks related to ε-martensite were very small and strongly overlapped with the reflections of γ-austenite, therefore the fraction of ε-martensite was not determined separately but rather it was included in the fraction of γ-austenite phase. This method of estimation is in agreement with the assumption that the ε-martensite is not a perfect hcp structure but rather considered as a heavily faulted fcc γ-austenite structure with a special arrangement of stacking faults [28]. The XRD patterns in Fig. 2 indicate the change of phase composition due to annealing. It can be seen that the amount of γ-austenite remained practically unchanged until the end of the exothermic peak at ~740 K. At the same time, in the endothermic peak the fraction of α'-martensite decreased from 74% to 15%, suggesting that this DSC peak corresponds to a reverse phase transformation from α′-martensite to γ-austenite. The change of the α′-martensite fraction and the most important parameters of the microstructure (grain size and dislocation density) can be followed in Fig. 3. At the highest annealing temperature (1000 K) applied in the current DSC analysis, the fraction of α′-martensite was reduced to ~7%, and this value is approximately the same as the fraction of α′-martensite observed in the initial material. It is worth noting that, despite the continuation of the reverse phase transformation between 950 and 1000 K, an endothermic signal was not observed. This apparent contradiction can be explained by the occurrence of simultaneous exothermic processes such as recovery and recrystallization at high temperatures. The lack of both exothermic and endothermic peaks in the temperature range of 950–1000 K suggests that there is an approximate equilibrium between the absorbed and released heats. In the next paragraph, the evolution of the microstructure during DSC annealing is studied.

The dislocation density in the main phase was determined by the XLPA method for the samples heated up to various temperatures. Fig. 3 shows that the major phase is α′-martensite in the HPT-processed state as well as in the beginning and at the end of the exothermic peak while at the end of the endothermic peak γ-austenite became the main phase. In the CMWP fitting method, the diffraction peaks reflected from phases other than the main phase were put into the background. Fig. 3 shows the dislocation density values (ρ) in the main phase for characteristic annealing temperatures. It is clear that the dislocation density practically remains unchanged during annealing up to the beginning of the exothermic DSC peak. In the exothermic DSC peak, the dislocation density decreased from $\sim 133 \times 10^{14}\ m^{-2}$ to $\sim 50 \times 10^{14}\ m^{-2}$. This suggests that recovery occurs in the temperature range corresponding to the first DSC peak. During the endothermic peak, the reduction of the dislocation density continued and at the end of this peak the dislocation density decreased to $\sim 13 \times 10^{14}\ m^{-2}$. The released heat related to this recovery could not be revealed in the thermogram as it was overwhelmed by the heat absorbed in the reverse martensitic phase transformation. After the endothermic peak (i.e., between 950 and 1000 K) the dislocation density further decreased to $\sim 6 \times 10^{14}\ m^{-2}$, however, the corresponding exothermic signal was not observed due to the simultaneous reverse martensitic phase transformation, as discussed above.

The CMWP fitting method enables a determination of the twin fault probability in fcc structures [37]. Therefore, at the end of the endothermic peak (at 950 K), the twin fault

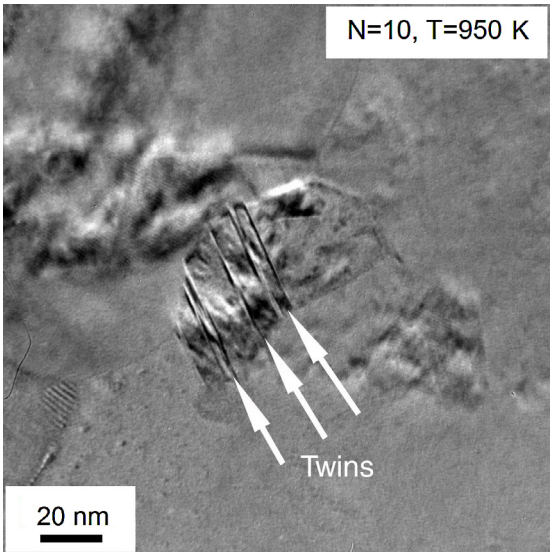

Fig. 4 – TEM images showing twin faults (indicated by white arrows) after annealing at 950 K of the sample processed by HPT for N = 10 turns.

probability (β_t) was also estimated in the main fcc γ-austenite phase. At 950 K, the twin fault probability was 0.6 ± 0.2%, which can be converted to a mean twin boundary spacing of 33 ± 15 nm using the equation $100\beta_t/d_{111}$ where d_{111} is the spacing between {111} lattice planes [27]. The presence of twin faults in the sample annealed at 950 K is confirmed by the TEM image in Fig. 4. The twin boundaries may be formed during HPT processing or in the reverse phase transformation from α′-martensite to γ-austenite. In the latter process, the internal stresses developed between the transformed and non-transformed volumes may be relaxed by twinning in the fcc phase due to the low SFE of 316L steel. In addition, the recrystallization of the HPT-processed microstructure at high temperatures may also yield the formation of twin boundaries since the low energy boundaries (such as twin boundaries) are preferred during recrystallization. This observation is in agreement with former studies which reported that the reversed γ-austenite obtained during annealing contained stacking faults and twins [38].

The evolution of the grain size during DSC annealing was determined by TEM. As illustrative examples, Fig. 5 shows dark field TEM images for the HPT-processed sample as well as for the states before the exothermic peak and after the endothermic peak. The average grain sizes determined from the TEM images are shown in Fig. 3. Immediately after HPT-processing the average grain size was ~45 nm, which increased to ~55 nm at the end of the exothermic peak. Therefore, the average grain size practically remained unchanged during the exothermic peak. Thus, it can be deduced that only a recovery of lattice defects without significant grain growth occurred in the exothermic peak. In the temperature range corresponding to the endothermic peak, the moderate grain growth continued and the grain size increased to ~70 nm at 950 K. Between 950 and 1000 K the grain size increased rapidly from ~70 to ~200 nm as revealed by the EBSD images shown in Fig. 6. The low and high angle grain boundaries (LAGBs and HAGBs) with misorientation angles lower and higher than 15° are indicated by green and black colors, respectively. The image in Fig. 6 indicates the abundance of HAGBs. In the next section, the change of the stored energy during DSC annealing will be calculated and compared with the experimentally determined heats released and absorbed in the exothermic and endothermic DSC peaks, respectively.

3.3. *Comparison of the change of stored energy with the heat released/absorbed during DSC*

The stored energy per unit mass for the sample processed by 10 turns of HPT is considered as the sum of the energies of the lattice defects (dislocations, grain boundaries and vacancies). The energy stored in the dislocations (E_{disl}) can be calculated from the dislocation density using the following equation [27,39,40]:

$$E_{disl} = A\frac{Gb^2\rho}{\rho_m}\ln\frac{1}{b\sqrt{\rho}}, \quad (2)$$

where G is the shear modulus (~82 GPa), b is the absolute value of the Burgers vector (~0.249 and ~0.254 nm for α′-martensite and γ-austenite, respectively), ρ is the dislocation density, ρ_m is the mass density ($\sim 8\times10^6\,g\,m^{-3}$), and A is a parameter depending on the material and the edge/screw character of dislocations. The magnitude of A is equal to

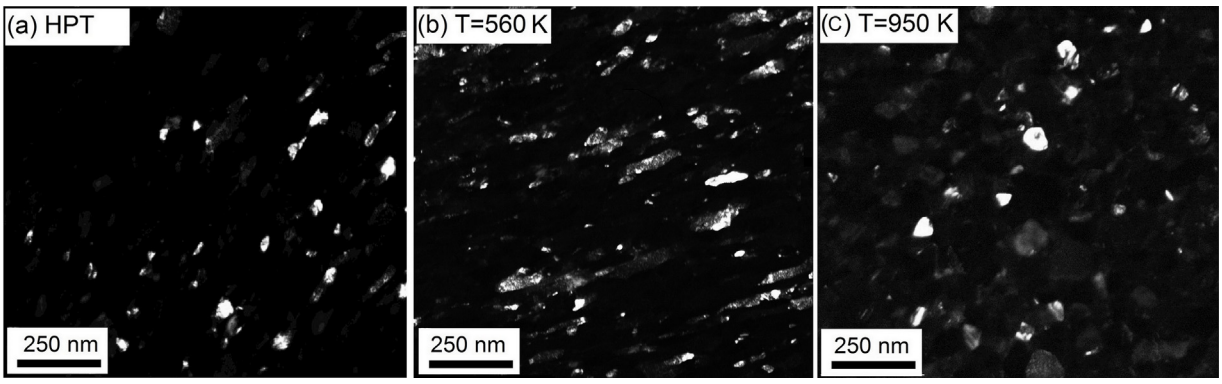

Fig. 5 – TEM images obtained for (a) the sample processed for N = 10 HPT turns and annealed up to (b) the beginning of the exothermic peak and (c) the end of the endothermic peak.

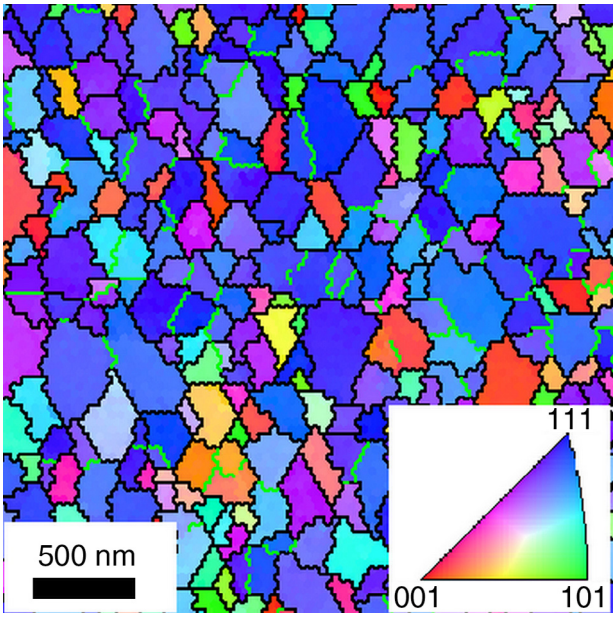

Fig. 6 – EBSD image taken on the specimen processed for 10 turns of HPT and then annealed up to 1000 K. The low and high angle grain boundaries are represented by green and black lines, respectively.

$(4\pi)^{-1}$ and $(4\pi(1-\nu))^{-1}$ for pure screw and pure edge dislocations, respectively, where ν is Poisson's ratio (taken as 0.33). The experimental value of the parameter q determined from XLPA describes the edge/screw character of dislocations. The theoretically calculated values of q for pure edge and screw dislocations for both fcc and bcc structures of 316L steel are listed in Table 1. For a mixed edge/screw dislocation character, the value of A can be estimated from the experimental value of q as [27,41]:

$$A = \frac{q - q_{edge}}{q_{screw} - q_{edge}} \frac{1}{4\pi} + \frac{q_{screw} - q}{q_{screw} - q_{edge}} \frac{1}{4\pi(1-\nu)}, \quad (3)$$

where q_{edge} and q_{screw} are the theoretically calculated values of q for pure edge and pure screw dislocations, respectively (see Table 1). The energy stored in the dislocations was calculated from the dislocation density and the value of q determined by XLPA. Immediately before the exothermic DSC peak, 74% of the material is α'-martensite and the value of E_{disl} is ~2.5 J/g in this phase. We assumed the same stored energy density in the minor γ-austenite phase in the HPT-processed material. Due to the recovery of the dislocation structure in the exothermic peak, E_{disl} was reduced to ~0.7 J/g. Therefore, the energy stored in dislocations has a contribution of ~1.8 J/g to the heat released in the exothermic DSC peak. The calculated values of the stored energy are summarized in Table 2.

The interfaces between grains and subgrains are classified into LAGBs and HAGBs. LAGBs usually consist of dislocations. XLPA measures the dislocation density in both LAGB boundaries and the interiors of the grains/subgrains, therefore the contribution of LAGBs to the stored energy is included in Eq. (2). The energy stored in HAGBs, E_{HAGB}, can be estimated using the following equation [42]:

$$E_{HAGB} = \frac{3\gamma_{GB}}{d\rho_m}, \quad (4)$$

where γ_{GB} is the average HAGB energy in 316L stainless steel (~0.6 J/m^2 [43]) and d is the average grain size. Table 2 shows that the change of E_{HAGB} in the exothermic DSC peak is small (~0.8 J/g) due to the very limited grain growth. Also, the grain size only moderately increases during annealing in the temperature range of the endothermic DSC peak. Thus, the change in E_{HAGB} is also small during this peak as shown in Table 3.

The sum of the changes of the energies stored in dislocations and HAGBs is ~2.6 J/g for the exothermic peak, which is much smaller than the heat released in this DSC peak (~4.9 J/g). The difference can be attributed to the annihilation of point defects, such as vacancies or vacancy clusters. The energy stored in vacancies (E_{vac}) can be calculated as the difference between the released heat measured in the exothermic DSC peak and the sum of the calculated stored energies. Table 2 shows the estimated value of E_{vac} for the vacancies annihilated in the exothermic peak. The vacancy concentration (c_v) can be calculated from E_{vac} as [40]:

$$c_v = E_{vac} \frac{M}{e_{vac} N_A}, \quad (5)$$

where e_{vac} is the formation energy of a vacancy in pure bcc iron (4.166×10^{-19} J [44]), N_A is Avogadro's number (6×10^{23} mol^{-1}) and M is the molar mass (56.2 g/mol). Using Eq. (5), the vacancy concentration annihilated in the exothermic DSC peak was obtained as $5.2 \pm 3.6 \times 10^{-4}$. It is noted that an exothermic peak with a small area (~1.3 J/g) was also detected for the initial material before HPT-processing. In this annealed and quenched sample, the grain size was large (~42 μm) and the

Table 2 – Comparison of the calculated stored energy and the heat released in the exothermic DSC peak for the sample processed by 10 HPT turns. E_{disl} and E_{HAGB} are the energies stored in dislocations and high-angle grain boundaries; E_{vac} is the energy stored in vacancies; H is the heat released in the exothermic DSC peak; c_v is the calculated vacancy concentration.

	Before the 1st DSC peak	After the 1st DSC peak	Difference
E_{disl} [J/g]	2.5 ± 0.2	0.70 ± 0.07	1.8 ± 0.3
E_{HAGB} [J/g]	4.8 ± 0.4	4.0 ± 0.4	0.8 ± 0.8
Sum [J/g]	7.3 ± 0.6	4.7 ± 0.5	2.6 ± 1.1
H [J/g]			4.9 ± 0.5
E_{vac} [J/g]			2.3 ± 1.6
c_v [10^{-4}]			5.2 ± 3.6

Table 3 – Comparison of the calculated stored energy and the heat released in the endothermic DSC peak for the sample processed by 10 HPT turns. E_{disl} and E_{HAGB} are the energies stored in dislocations and high-angle grain boundaries; E_{vac} is the energy stored in vacancies; H is the heat released in the exothermic DSC peak; $\Delta(E_{disl}+E_{HAGB})$ is the change of the sum of dislocation and grain boundary stored energies during the exothermic DSC peak; $E_{martensite}$ is the energy of the reverse martensitic phase transformation.

	Before the 2nd DSC peak	After the 2nd DSC peak	Difference
E_{disl} [J/g]	0.70 ± 0.08	0.30 ± 0.03	0.40 ± 0.11
E_{HAGB} [J/g]	4.0 ± 0.4	3.2 ± 0.4	0.8 ± 0.8
Sum [J/g]	4.70 ± 0.48	3.50 ± 0.43	1.2 ± 0.9
H [J/g]			−5.7 ± 0.6
H-$\Delta(E_{disl}+E_{HAGB})$ [J/g]			−6.9 ± 1.5
Change of austenite fraction			0.59 ± 0.06
$E_{martensite}$ [J/g]			−11.7 ± 3.5

material was practically free of dislocations, therefore the energy measured in the exothermic DSC peak can be related only to the annihilation of vacancies. Accordingly, the vacancy concentration calculated from Eq. (5) is about 2.9×10^{-4}.

During the endothermic DSC peak, there is a reversion from α′-martensite to γ-austenite which absorbs heat while the annihilation of dislocations and grain growth leads to a heat release. The heat absorbed in the endothermic DSC peak was −5.7 J/g. The energy of the reverse martensitic phase transformation can be estimated as the difference between the measured heat absorbed in the endothermic peak and the sum of the stored energies for dislocations and HAGBs. Table 3 shows that the annihilation of dislocations and grain growth in the main γ-austenite phase resulted in a change of stored energy of ~1.2 J/g. We assumed the same change in the stored energy for the minor α′-martensite phase. Therefore, the energy of the reverse martensitic phase transformation was obtained as −6.9 J/g. Taking into account the change of the austenite fraction in the temperature range of the endothermic peak, the energy required for α′-martensite reversion was estimated as −11.7 ± 3.5 J/g.

4. Discussion

The vacancy concentration calculated for both the initial material and the sample processed by HPT is of the order of 10^{-4}. In thermal equilibrium, such a large vacancy concentration can only be achieved at very high temperatures. In the case of the initial undeformed material, this very high vacancy concentration can be explained by the applied thermal treatment of this sample. In fact, the initial 316L specimen was prepared by annealing at 1373 K for 1 h and then quenching to RT. Therefore, the high concentration of vacancies at 1373 K was most probably frozen during quenching of the initial sample. As the vacancy diffusion in coarse-grained materials is very slow at RT, therefore the high vacancy concentration in the quenched material can be preserved for long times. HPT-processing yielded further enhancement in the vacancy concentration as SPD produces a high amount of excess vacancies. Earlier studies showed that the excess vacancy concentration in pure Cu and Ni samples processed by HPT at RT can achieve the values of $0.9–20 \times 10^{-4}$ [45,46]. The value of c_v obtained for the present 316L steel is in agreement with these earlier results. It is noted that former studies [45,46] revealed that in SPD-processed metallic materials vacancies tend to form clusters with decreasing SFE. For instance, in 99.95% purity Cu the clusters consist of 4–9 vacancies [45]. As 316L steel has a low SFE, therefore the vacancies annihilated in the exothermic DSC peak were most probably arranged into clusters during HPT or in the beginning of the DSC scan. It should also be noted that the change of the density of twin-faults during annealing probably influences the heat released and absorbed during the DSC experiments. However, the very low SFE of 316L steel yields a low twin-fault energy, therefore the effect of twin-faults on the stored energy can be neglected.

In the analysis of the change of the stored energy during the endothermic peak, we assumed that the majority of vacancies were annihilated in the first DSC peak, therefore only the heat released due to dislocation annihilation and grain growth was considered. Thus, the energy of the reverse martensitic phase transformation may be slightly larger than the calculated value of −11.7 ± 3.5 J/g. This phase transformation energy agrees within the experimental error with the values obtained in former studies. For instance, it was documented that the reverse phase transformation in cold-worked AISI 304 steel occurred in the temperature range between 740 and 820 K with a martensite reversion energy of about −8 J/g [47], and a similar value was obtained for 16Cr–10Ni steel (−8.8 J/g) [16]. It is noted that the reverse phase transformation energy depends on the chemical composition of steel. For instance, the enthalpy of phase transformation from bcc to fcc structure in pure iron was found to be −16 J/g [48]. Therefore, it can be concluded that the reversion energy of −11.7 J/g determined in this study is in a reasonable agreement with the literature.

5. Summary and conclusions

1. The change of the stored energy during annealing of a nanocrystalline 316L stainless steel was calculated and compared with the heat released and absorbed during DSC experiments. The nanostructure was processed from an annealed and quenched material by HPT applied for 10 turns at RT. In the DSC thermogram obtained for the HPT-processed sample, two characteristic peaks were observed. The first was an exothermic peak which was related to the annihilation of lattice defects (dislocations and vacancies). During this recovery, the phase composition remained practically unchanged and the average grain size was only slightly increased. From the comparison of the heat

released in the exothermic peak and the change of energies stored in dislocations and HAGBs, the concentration of annihilated vacancies was determined as $\sim 5.2 \times 10^{-4}$. An exothermic peak was also detected for the initial material, which was related to the vacancies frozen in the sample during quenching. The concentration of these excess vacancies was also as high as 2.9×10^{-4}.

2. The second peak between 740 and 950 K in the DSC thermogram was an endothermic peak which was caused primarily by the reverse phase transformation from α'-martensite to γ-austenite. During this second peak, besides the phase transformation, the annihilation of dislocations and the grain growth continued. Subtracting the heat released due to these recovery processes from the heat absorbed in the endothermic peak, the energy of the reverse phase transformation was estimated as -11.7 J/g. This value is in a reasonable agreement with the values reported in the literature.
3. Although the endothermic peak finished at $\sim$950 K, the reverse phase transformation continued up to $\sim$1000 K. In this temperature range, the energy required for α'-martensite reversion was in an approximate balance with the energy released due to recovery and grain growth, therefore a DSC signal was not detected. The HPT-processed 316L stainless steel annealed to 1000 K exhibited a small grain size of $\sim$200 nm and a considerable dislocation density of $\sim 6 \times 10^{14}$ m^{-2}, which indicates the good thermal stability of this material.

Conflicts of interest

The authors declare no conflicts of interest.

Acknowledgments

This research was presented at the 3rd Pan American Materials Congress held as part of the TMS Annual Meeting in San Diego, California, on February 27–March 2, 2017. The authors are grateful to Mr. Alajos Ö. Kovács and Mr. Gábor Varga for DSC and EBSD investigations, respectively. This research was supported by the Hungarian Scientific Research Fund, OTKA, Grant no. K-109021. Two of the authors (YH and TGL) were supported by the European Research Council under ERC Grant Agreement No. 267464-SPDMETALS.

REFERENCES

[1] Gotman I. Characteristics of metals used in implants endourology. J Endourol 1997;11(6):383–9.
[2] Lucas GL, Cooke FW, Friis EA. Orthopaedic alloys. New York: Springer Science + Business Media; 1999. p. 198–212 [Chapter 14].
[3] Kim W, Yoon S, Ryu W, Lee C. Application of minimum commitment method for predicting long-term creep life of type 316LN stainless steel. J Korean Inst Metals Mater 2008;46(3):118–24.
[4] Kim Y, Kim Y, Kim D, Kim S, Nam W, Choe H. Effects of hydrogen diffusion on the mechanical properties of austenite 316L steel at ambient temperature. Mater Trans 2011;52(3):507–13.
[5] Mine Y, Horita Z, Murakami Y. Effect of hydrogen on martensite formation in austenitic stainless steels in high-pressure torsion. Acta Mater 2009;57(10):2993–3002.
[6] Scheriau S, Zhang Z, Kleber S, Pippan R. Deformation mechanisms of a modified 316L austenitic steel subjected to high pressure torsion. Mater Sci Eng: A 2011;528(6):2776–86.
[7] Silva PMO, Abreu HFG, Albuquerque VHC, Neto PL, Tavares JMRS. Cold deformation effect on the microstructures and mechanical properties of AISI 301LN and 316L stainless steels. Mater Des 2011;32(2):605–14.
[8] Gubicza J, El-Tahawy M, Huang Y, Choi H, Choe H, Lábár JL, et al. Microstructure, phase composition and hardness evolution in 316L stainless steel processed by high-pressure torsion. Mater Sci Eng: A 2016;657:215–23.
[9] Valiev RZ, Estrin Y, Horita Z, Langdon TG, Zehetbauer MJ, Zhu YT. Producing bulk ultrafine-grained materials by severe plastic deformation. JOM 2006;58(4):33–9.
[10] Zhilyaev AP, Langdon TG. Using high-pressure torsion for metal processing: fundamentals and applications. Progr Mater Sci 2008;53(6):893–979.
[11] Valiev RZ, Zhilyaev AP, Langdon TG. Bulk nanostructured materials: fundamentals and applications. New Jersey: John Wiley & Sons, Inc. Hoboken; 2014.
[12] Langdon TG. Twenty-five years of ultrafine-grained materials: achieving exceptional properties through grain refinement. Acta Mater 2013;61(13):7035–59.
[13] Abreu HFG, Carvalho SS, Neto PL, Santos RP, Freire VN, Silva PMO, et al. Deformation induced martensite in an AISI 301LN stainless steel: characterization and influence on pitting corrosion resistance. Mater Res 2007;10(4):359–66.
[14] Guy KB, Butler EP, West DRF. Reversion of bcc: α' martensite in Fe–Cr–Ni austenitic stainless steels. Metal Sci 1983;17(4):167–76.
[15] Roland T, Retraint D, Lu K, Lu J. Enhanced mechanical behavior of a nanocrystallised stainless steel and its thermal stability. Mater Sci Eng: A 2007;445–446:281–8.
[16] Somani MC, Juntunen P, Karjalainen LP, Misra RDK, Kyröläinen A. Enhanced mechanical properties through reversion in metastable austenitic stainless steels. Metall Mater Trans: A 2009;40(3):729–44.
[17] Forouzan F, Najafizadeh A, Kermanpur A, Hedayati A, Surkialiabad R. Production of nano/submicron grained AISI 304L stainless steel through the martensite reversion process. Mater Sci Eng: A 2010;527(27–28):7334–9.
[18] El-Tahawy M, Huang Y, Choi H, Choe H, Lábár JL, Langdon TG, et al. High temperature thermal stability of nanocrystalline microstructure in 316L stainless steel processed by high-pressure torsion. Mater Sci Eng: A 2017;682:323–31.
[19] Almathami A, Goodall G, Brochu M. Crystal structure, transformation and thermal stability of nanostructured 316LSS alloyed with 2 and 6 wt% aluminum. Mater Sci Eng: A 2010;527(21–22):6020–7.
[20] Takaki S, Tomimura K, Ueda S. Effect of pre-cold-working on diffusional reversion of deformation induced martensite in metastable austenitic stainless steel. ISIJ Int 1994;34(6):522–7.
[21] Tomimura K, Takaki S, Tokunaga Y. Reversion process of deformatien induced martensite to austenite in metastable austenitic stainless steels. Tetsu-to-Hagane 1988;74(8):1649–56.
[22] Tomimura K, Takaki S, Tokunaga Y. Reversion mechanism from deformation induced martensite to austenite in metastable austenitic stainless steels. ISIJ Int 1991;31(12):1431–7.

[23] Schramm RE, Reed RP. Stacking fault energies of seven commercial austenitic stainless steels. Metall Trans: A 1975;6(7):1345–51.
[24] Vitos L, Nilsson JO, Johansson B. Alloying effects on the stacking fault energy in austenitic stainless steels from first-principles theory. Acta Mater 2006;54(14):3821–6.
[25] Rhodes CG, Thompson AWM. The composition dependence of stacking fault energy in austenitic stainless steels. Metall Trans: A 1977;8(12):1901–6.
[26] Miodowni AP. The calculation of stacking fault energies in Fe–Ni–Cr alloys. Calphad 1978;2(3):207–26.
[27] Gubicza J. Defect structure in nanomaterials. Cambridge, UK: Woodhead Publishing Ltd.; 2012.
[28] Guy K, Butler EP, West DRF. ε and α' martensite formation and reversion in austenitic stainless steels. J Phys Colloq 1982;43(C4):575–80.
[29] Sun C, Yang Y, Liu Y, Hartwig KT, Wang H, Maloy SA, et al. Thermal stability of ultrafine grained Fe–Cr–Ni alloy. Mater Sci Eng: A 2012;542:64–70.
[30] Figueiredo RB, Cetlin PR, Langdon TG. Using finite element modeling to examine the flow processes in quasi-constrained high-pressure torsion. Mater Sci Eng: A 2011;528(28):8198–204.
[31] Figueiredo RB, Pereira PHR, Aguilar MTP, Cetlin PR, Langdon TG. Using finite element modeling to examine the temperature distribution in quasi-constrained high-pressure torsion. Acta Mater 2012;60(6–7):3190–8.
[32] Ribárik G, Gubicza J, Ungár T. Correlation between strength and microstructure of ball-milled Al–Mg alloys determined by X-ray diffraction. Mater Sci Eng: A 2004;387–389(2–3):343–7.
[33] Borbély A, Dragomir-Cernatescu J, Ribárik G, Ungár T. Computer program ANIZC for the calculation of diffraction contrast factors of dislocations in elastically anisotropic cubic, hexagonal and trigonal crystals. J Appl Crystal 2003;36:160–2.
[34] Mangalick ME, Fiore NF. Orientation dependence of dislocation damping and elastic constants in Fe–18Cr–Ni single crystals. Trans Metall Soc AIME 1968;242(11):2363–4.
[35] Baudouin J, Monnet G, Perez M, Domain C, Nomoto A. Effect of the applied stress and the friction stress on the dislocation dissociation in face centered cubic metals. Mater Lett 2013;97:93–6.
[36] Yeddu HK, Razumovskiy VI, Borgenstam A, Korzhavyi PA, Ruban AV, Agren J. Multi-length scale modeling of martensitic transformations in stainless steels. Acta Mater 2012;60(19):6508–17.
[37] Balogh L, Ribárik G, Ungár T. Stacking faults and twin boundaries in fcc crystals determined by X-ray diffraction profile analysis. J Appl Phys 2006;100(2), 23512-1–10.
[38] Smith H, West DRF. The reversion of martensite to austenite in certain stainless steels. J Mater Sci 1973;8(10):1413–20.
[39] Bever MB, Holt DL, Titchener AL. The stored energy of cold work. Progr Mater Sci 1973;17:5–177.
[40] Schafler E, Steiner G, Korznikova E, Kerber M, Zehetbauer MJ. Lattice defect investigation of ECAP-Cu by means of X-ray line profile analysis, calorimetry and electrical resistometry. Mater Sci Eng: A 2005;(410–411):169–73.
[41] Gubicza J, Dobatkin SV, Khosravi E, Kuznetsov AA, Lábár JL. Microstructural stability of Cu processed by different routes of severe plastic deformation. Mater Sci Eng: A 2011;528(3):1828–32.
[42] Humphreys FJ, Hatherly M. Recrystallization and related annealing phenomena. Oxford, UK: Elsevier; 2004.
[43] Barr CM, Vetterick GA, Unocic KA, Hattar K, Bai X-M, Taheri ML. Anisotropic radiation-induced segregation in 316L austenitic stainless steel with grain boundary character. Acta Mater 2014;67:145–55.
[44] Ramunni VP, Rivas AMF. Diffusion behavior of Cr diluted in bcc and fcc Fe: classical and quantum simulation methods. Mater Chem Phys 2015;162:659–70.
[45] Setman D, Schafler E, Korznikova E, Zehetbauer MJ. The presence and nature of vacancy type defects in nanometals detained by severe plastic deformation. Mater Sci Eng: A 2008;493(1–2):116–22.
[46] Cizek J, Janecek M, Srba O, Kuzel R, Barnovska Z, Prochazka I, et al. Evolution of defects in copper deformed by high-pressure torsion. Acta Mater 2011;59(6):2322–9.
[47] Haebner F, Plaut R, Padilha AF. Separation of static recrystallization and reverse transformation of deformation-induced martensite in an austenitic stainless steel by calorimetric measurements. ISIJ Int 2003;43(9):1472–4.
[48] Chen Q, Sundman B. Modeling of thermodynamic properties for Bcc, Fcc, liquid, and amorphous iron. J Phase Equilib 2001;22(6):631–44.